Human mitochondrial DNA variants influence telomere length: evidence from a transmitochondrial cybrid model

Manon Mahieu[1,#], Jean-Philippe Defour[2,3,#], Barbara Mathieu[4], Elena Richiardone[5], Isaac Heremans[6], Elisa Fabiole[7,8], Gabriel Levy[2], Gabriel Le Berre[1], Isabelle Scheers[9], Bénédicte Brichard[2], Thierry Arnould[10], Patrick Revy[7], Guido Bommer[6], Bernard Gallez[4], Cyril Corbet[5,11*] & Anabelle Decottignies[1,*]

[1] Genetic & Epigenetic Alterations of Genomes, de Duve Institute, UCLouvain, Brussels, Belgium

[2] Cliniques Universitaires Saint-Luc, UCLouvain, Brussels, Belgium

[3] Current address: CHC Liège, Liège, Belgium

[4] Biomedical Magnetic Resonance Unit, Louvain Drug Research Institute, UCLouvain, 1200 Brussels, Belgium

[5] Pole of Pharmacology and Therapeutics, Institut de Recherche Expérimentale et Clinique, UCLouvain, Brussels, Belgium

[6] Biochemistry, de Duve Institute, UCLouvain, Brussels, Belgium

[7] Laboratory of Genome Dynamics in Human Diseases, Equipe Labellisée Ligue 2026, INSERM UMR 1163, Imagine Institute, Paris, France

[8] Université Paris Cité, Imagine Institute, Paris, France

[9] Pediatric gastroenterology and hepatology unit, Cliniques universitaires Saint-Luc, Université catholique de Louvain, Brussels, Belgium

[10] Laboratory of Biochemistry and Cell Biology, NAmur Research Institute for LIfe Sciences (NARILIS), UNamur, Namur, Belgium

[11] WEL Research Institute, Wavre, Belgium

# These authors contributed equally

*Corresponding authors: Anabelle Decottignies, Cyril Corbet

Email: anabelle.decottignies@uclouvain.be, cyril.corbet@uclouvain.be

Author Contributions: M.M., J.-P.D. and A.D. generated the Flow-FISH curves. G.L., I.S., B.B. and A.D. recruited volunteers and helped collecting blood. M.M., B.M. and B.G. contributed to ROS measurement. M.M., E.R. and C.C. contributed to OCR and ETC complex activity measurement and to glycolytic flux evaluation. I.H. and G.B. contributed to metabolite analyses. E.F. and P.R. contributed to ddTRAP analyses. M.M. and T.A. contributed to transmitochondrial cybrid formation. G.L.B. contributed to PAR-FISH analysis. M.M. performed TRF, TeSLA, RT-qPCR, IF/FISH and qPCR analyses. A.D. and C.C. designed and supervised the study. A.D. wrote the paper.

Competing Interest Statement: The authors declare no conflicts of interest.

Keywords: Mitochondrial genome, Telomeres, Telomere length inheritance, Oxidative stress, Complex I

This PDF file includes:

Main Text
Figures 1 to 4

Abstract

Telomere shortening is a hallmark of aging, yet telomere length (TL) varies considerably among individuals and is strongly influenced by inheritance. In mice, efficient mitochondrial function-characterized by low reactive oxygen species (ROS) production-is critical for telomere elongation during early embryogenesis. Since mitochondrial DNA (mtDNA) encodes several subunits of the electron transport chain, it may influence TL at birth by regulating mitochondrial function *in utero*. To explore the relationship between mtDNA and TL, we used a transmitochondrial cybrid approach, introducing mitochondria from donor platelets with varying telomere lengths into mtDNA-depleted cells. This revealed an inverse correlation between donor blood TL and mitochondrial ROS levels measured in the resulting cybrids. Under the specific conditions of cybrid formation, which involve a metabolic shift from glycolysis to oxidative phosphorylation, mtDNA variants associated with reduced complex I (CI) activity induced rapid telomere shortening, further implicating mitochondrial metabolism in TL regulation. Notably, this effect was prevented by antioxidant treatment and supplementation with NAD^+ precursors, supporting a critical role for CI in sustaining PARP1 activity through maintenance of the NAD^+/NADH balance to preserve telomere integrity under acute

oxidative stress. Collectively, these findings suggest that specific mtDNA variants may contribute to the maintenance of long telomeres in humans by enhancing mitochondrial fitness, thereby highlighting potential therapeutic opportunities for mitochondrial replacement strategies.

Significance Statement

Telomere length at birth influences aging trajectories and disease risk later in life, yet the mechanisms governing this trait remain incompletely understood. Using a transmitochondrial cybrid approach, we show that single-nucleotide variants in the mitochondrial genome of healthy donors directly affect mitochondrial metabolism and reactive oxygen species production. In addition, mitochondrial ROS levels measured in cybrids inversely correlate with blood cell telomere length in donors. Mitochondrial DNA variants associated with reduced complex I activity promote telomere shortening during an i*n vitro* metabolic shift toward oxidative phosphorylation, an effect that is reversed by antioxidant treatment or NAD^+ precursor supplementation. Together, these findings establish a direct link between mitochondrial genetics, redox homeostasis, and telomere maintenance in human cells.

Introduction

Telomeres form protective caps at chromosome ends thanks to the binding of a six-member protein complex termed shelterin (1). With cell divisions, telomeres of normal somatic cells progressively shorten, a process that likely contributes to cellular aging and the development of various age-related pathologies (2,3). Accordingly, cohort studies established that shorter leucocyte telomere length (TL) was associated with a higher risk of diseases affecting specific organs, such as the lung or the liver, and an increased incidence of esophageal cancer, as well as lymphoid and myeloid leukemia (4).

While aging is a key determinant of TL, genetic variation also plays a significant role in the variability of leukocyte TL among healthy individuals, as evidenced by the identification of nuclear genomic SNPs associated with TL (5). Heritability estimates for human TL reach 82% (6). Consistently, TL in the zygote appears to play a key role in determining TL later in life (5), indicating that it is largely established during early embryonic development. Telomere length resetting during embryogenesis is a telomerase-dependent process that occurs at the morula-to-blastocyst transition (7). Recent findings in mice show that experimentally disrupting mitochondrial function in zygotes significantly impairs telomere elongation between the 8-cell and blastocyst stages, ultimately leading to shorter telomeres in the offspring (8). Similar outcomes have been observed in offspring from reproductively aged or obese female mice -two conditions known to compromise oocyte

92 mitochondrial integrity (8). Collectively, these findings underscore the critical role of proper
93 mitochondrial function in telomere regulation during embryogenesis. Further evidence comes from
94 individuals with mitochondrial disorders such as MELAS syndrome and Leber's hereditary optic
95 neuropathy (LHON). These individuals exhibit significantly shorter leukocyte telomeres at birth,
96 likely reflecting impaired TL establishment during early development (9).

97 While damaged mitochondria are associated with shorter TL in mouse embryos and may impair TL
98 regulation in patients with mitochondrial diseases (9), the impact of naturally occurring
99 mitochondrial genome SNPs on TL remains largely unexplored. With a total of 29 haplogroups and
100 a myriad of subhaplogroups characterized by distinct variants compiled in the Mitomap database
101 (10), human mtDNA genomes display large heterogeneity. Some variants within the coding regions
102 of mtDNA, such as the NADH dehydrogenase subunits (ND1, 2, 3, 4, 4L and 5) of complex I (CI),
103 Cytochrome b, the COXI, II and III subunits of CIV or the ATP6 and 8 subunits of the ATP synthase
104 (CV) lead to distinct ETC properties that impact mitochondrial metabolism and ROS production. In
105 line with the hypothesis that the mitochondrial genome may contribute to the observed stronger
106 maternal influence on TL at birth (6,11) -given that mtDNA is maternally inherited-, we hypothesized
107 that non-pathogenic variation in the mtDNA sequence could affect TL.

108 Building on reference curves for TL in the Belgian population, obtained through fluorescence *in situ*
109 hybridization (FISH) combined with flow cytometry (Flow-FISH), we identified mtDNA variants
110 associated with either very long or short leukocyte TL. We leveraged a transmitochondrial cybrid
111 approach to directly test the effects of these mtDNA variants on mitochondrial function in mtDNA-
112 depleted recipient cells and uncovered an inverse relationship between leukocyte TL in the donors
113 and mitochondrial ROS levels measured in the cybrids. Our results further highlight the critical role
114 of mtDNA-encoded CI activity in sustaining NAD^+ metabolism and telomere integrity, particularly
115 under oxidative stress conditions arising during the metabolic transition from glycolysis to oxidative
116 phosphorylation in early cybrid development. Collectively, these findings reinforce the link between
117 mtDNA-encoded mitochondrial function and telomere regulation in human cells.

118

119 **Results**

120 **Establishment of reference curves for TL using Flow-FISH**

121 To establish reference curves for TL in Belgium, we applied the gold standard Flow-FISH approach
122 (12) on leukocytes isolated from a cohort of 491 healthy donors aged 7 days to 99 years old.
123 Percentile curves for TL in lymphocytes (Fig 1A) and granulocytes (Fig 1B) were comparable to
124 those obtained previously (13,14) (Fig S1A) and showed large heterogeneity among individuals of

125 similar age. Although still controversial, obesity may negatively impact TL (5,15). In our cohort,
126 average BMI was not statistically different between donors with telomeres below the 5th or above
127 the 90th percentile (Fig S1B). Given previous evidence supporting a stronger maternal inheritance
128 of TL in humans (6,11), with similar trend observed in birds (16), we sought to investigate the
129 potential contribution of the human mitochondrial genome to TL heterogeneity. To this end, we
130 selected individuals with long, average or short telomeres from our Flow-FISH curves (Fig 1C). All
131 were of European origin, thus excluding a possible bias linked to African ethnic groups (5), and the
132 seven donors belonged to distinct mitochondrial subhaplogroups (Fig 1D). Strikingly, donor #6, with
133 lymphocyte telomeres at the 95th percentile, turned out to belong to the K1a subhaplogroup that
134 encompasses the centenarian-enriched A177T variant (m.G9055>A) in the ATP6 subunit of ATP
135 synthase (CV) (17,18) with an allele frequency of 5.4% in Mitomap database (Fig 1D).
136
137 **Distinct mitochondrial genomes differently modulate TL in transmitochondrial cybrids**

138 To evaluate the impact of distinct mitochondrial genomes on TL in human cells, we used a
139 transmitochondrial cybrid strategy in which mtDNA-depleted Rho^0 (ρ^0) cells are fused with donor
140 platelets, thereby restoring functional mitochondria carrying donor-specific mtDNA variants (19).
141 The presence of variants in cybrids was checked by sequencing and mtDNA content was evaluated
142 by qPCR (Fig S2). Southern blot analysis revealed that telomeres in 143B ρ^0 cells were shorter
143 than in parental 143B cells (Fig 2A). To rule out clonal artifacts, mtDNA depletion was
144 independently repeated, and multiple ρ^0 clones were isolated, all of which exhibited a consistent
145 reduction in TL (Fig S3A). This telomere shortening was not associated with decreased expression
146 of the telomerase subunits h*TR* or h*TERT* (Fig S3B), but correlated with a reduction in telomerase
147 activity measured *in vitro* using cell extracts (Fig S3C).

148 In line with a role for mitochondrial function in supporting telomerase activity, fusion of 143B ρ^0 cells
149 with platelets from donors #6 and #7 (Cyb6 and 7) restored telomerase activity and rescued TL in
150 ρ^0 cells to levels comparable to those of parental 143B cells (Fig 2A-B and Fig S3D). Telomere
151 elongation in these cybrids was accompanied by a reduced frequency of short telomeres, as
152 assessed by TeSLA (Fig S3E). Unexpectedly, TL was not restored in Cyb1-5 cybrids. Instead,
153 fusion with platelets from donors #1 and #2 induced a marked and reproducible telomere shortening
154 in ρ^0 recipient cells (Fig 2A and Fig S3D). This effect was not associated with reduced telomerase
155 activity or decreased h*TR* or h*TERT* transcript levels, but rather with pronounced telomeric damage
156 and telomere fusions following fusion (Fig 2B-E).

157 Together, these findings demonstrate that mitochondrial DNA sequence variation exerts a strong
158 influence on telomere length in 143B ρ^0 recipient cells, ranging from telomere elongation to severe
159 shortening.

160 **Low complex I activity shortens the telomeres of ρ^0 recipient cells**

161 We next investigated why different mtDNA sequences exerted such divergent effects on TL in 143B
162 ρ^0 recipient cells. When mitochondria are replenished in ρ^0 cells during the formation of
163 transmitochondrial cybrids, a shift from glycolysis to OXPHOS occurs (Fig S4A-B) and cells need
164 to adapt to this metabolic change. Complex I (CI) plays a crucial role in regulating the NAD^+/NADH
165 balance and this is crucial for the activity of NAD^+-dependent poly (ADP-ribose) polymerase 1)
166 (PARP1) repair enzyme, an enzyme required for the repair of telomeres undergoing oxidative
167 stress in cultured cells (20-22). We thus hypothesized that optimal levels of CI activity may be
168 required for telomere protection in cells experiencing acute oxidative stress during the *in vitro*
169 metabolic shift before cellular adaptation. Consistent with this, we found significantly lower CI
170 activity in Cyb1 and Cyb2 cybrids (Fig 3A) and a strong positive correlation between TL measured
171 in the cybrids at the first passages and CI activity (Fig 3B). Supporting a lower CI activity in in Cyb1
172 and Cyb2 cybrids, we noticed a significant up-regulation of the NAD^+ salvage pathway genes
173 *NAMPT* and *NAPRT1*, likely reflecting a compensatory mechanism (Fig 3C).

174 Building on the idea that, in the context of lower CI activity, telomeres may not be able to resist
175 oxidative stress-induced shortening, we repeated the fusion of donor #2's platelets to 143B ρ^0 cells
176 in the presence of N-acetyl-L-cysteine (NAC) antioxidant and/or nicotinamide riboside (NR), a
177 precursor of NAD^+. Strikingly, while telomeres were shortened in all clones (5/5) selected from
178 cybrids obtained in the presence of N-acetyl-L-alanine (NAA) used as control, only one out of the
179 eight selected cybrids obtained in the presence of both NAC and NR showed telomere shortening
180 (Fig 3D-E). Treatment with either NAC or NR alone showed intermediate phenotype (Fig 3D-E).
181 The detection of telomeric parylation signals further supported a role for NAD^+-dependent PARP1
182 activity in repairing oxidative damage at shortened telomeres during the process of cybrid formation
183 (Fig 3F).

184 Altogether, we propose that the *in vitro* process of cybrid formation exacerbates the impact of low
185 CI activity on telomeres during the acute oxidative stress linked to a metabolic shift from glycolysis
186 to OXPHOS.

187 **Lymphocyte TL inversely correlates with ROS levels in transmitochondrial cybrids**

188 Having identified CI activity as a strong regulator of TL during *in vitro* cybridisation, we asked
189 whether mtDNA-encoded CI activity could also account for the differences in TL observed in
190 donors' blood cells. However, analysis of age-adjusted lymphocyte TL *versus* CI activity revealed
191 no association between these parameters (Fig 4A).

192 In mouse oocytes, impaired mitochondrial function, associated with elevated mitochondrial ROS
193 production, adversely affects telomere elongation (8). In human cells, experimentally induced
194 mitochondrial dysfunction was also reported to lead to telomere damage through the production of
195 ROS (23). We therefore tested whether human mitochondrial genomes, through their impact on
196 ROS levels, may modulate TL in blood cells. As transmitochondrial cybrids receive the donors'
197 mitochondria but no other genetic information, this cellular model allows to specifically assess the
198 impact of the mitochondrial genome on ROS production. Mitochondrial superoxide production was
199 measured by electron paramagnetic resonance (24) in clones #1 of all cybrids (Fig 4B). Differences
200 in ROS levels across the cybrids were not linked to distinct changes in oxidative *vs* glycolytic
201 metabolism in the cybrids that were characterized by similar lactate/glucose and ATP/ADP ratios
202 (Fig S5A-B). Strikingly, ROS levels in the cybrids inversely correlated with the age-adjusted TL
203 measured by Flow-FISH in the corresponding donors' lymphocytes (Fig 4C). Elevated levels of
204 ROS were notably detected in Cyb3 cybrid. The mtDNA from donor #3 harbors the extremely rare
205 F63L variant (m.T6090>C; Mitomap frequency: 0.002%) in the COX1 subunit, located within a
206 transmembrane helix in close proximity to the heme A group and associated with reduced CIV
207 efficiency (Fig 4D and Fig S6). Together, these findings support a role for mitochondrial ROS in
208 human TL regulation *in vivo*.

209 **Rare mtDNA variants may account for the maternal inheritance of long telomeres**

210 To further assess the relevance of our findings to a potential role of mitochondria in TL inheritance
211 in humans, we searched for evidence of maternal inheritance of TL within families. Such analyses
212 are most informative in families with extremely long (>P90) or short (<P10) telomeres. We therefore
213 focused on three individuals with lymphocyte TL above the 90th percentile: donors #1, #6, and #7
214 (Fig 1C).

215 Despite donor #1 exhibiting lymphocyte TL at the 99th percentile, TL in lymphocytes from both of
216 this donor's children was close to the 50th percentile or only slightly above, arguing against a
217 dominant maternal inheritance of the exceptionally long telomeres observed in donor #1 (Fig 4E).
218 Donor #6 belongs to the K1a subhaplogroup Identified by the MitoAging project as one of the four
219 mtDNA variants significantly associated with longevity, with the A177T variant also showing
220 protective effect against Parkinson's disease (25). Although we could not assess TL in donor #6's
221 progeny, as she does not have children, the fact that her mother showed telomeres at the 90th

222 percentile and that two European male donors, identified in independent cohorts (26) as having
223 telomeres at, respectively, the 97.5th and above the 99th percentile (Fig 4E), were found to display
224 K1a mtDNA, support the notion that this subhaplogroup is associated with long telomere
225 inheritance. This led us to screen additional unrelated donors with varying TL for the presence of
226 the m.G9055>A variant. The variant was identified in 1 of 11 donors with lymphocyte TL below the
227 50th percentile, 2 of 26 donors with TL between the 50th and 90th percentiles, and 3 of 13 donors
228 with TL at or above the 90th percentile (Fig 4F and Fig S7), suggesting a trend toward higher
229 frequency of the m.G9055>A (ATP6 A177T) variant among individuals with lymphocyte TL at or
230 above the 90th percentile (p=0.153).

231 Donor #7 does not belong to the K1a haplogroup; nevertheless, both her mother and her daughter
232 exhibited telomere lengths at the 95th and near the 90th percentile, respectively (Fig 4E). In contrast,
233 the telomere lengths of her husband and her father were slightly above the 10th and around the 50th
234 percentile, respectively (Fig 4E). These findings pointed to a maternal inheritance pattern
235 associated with the H1b1e mtDNA subhaplogroup, identified through blood sequencing in these
236 women but not previously linked to longevity. While the causal link between the rare m.A3796>G
237 variant in donor #7 (ND1 T164A, CI) and the long telomere phenotype remains to be determined,
238 this variant was absent in all 49 unrelated donors with varying telomere lengths that we screened.

239 Collectively, these findings support the idea that multiple mitochondrial genome SNPs may
240 contribute to the inheritance of telomere length.

241

242 **Discussion**

243

244 While long telomeres are often viewed as markers of good cellular health, shorter leukocyte TL is
245 linked to a higher risk of diseases affecting organs like the lungs and liver, as well as various
246 cancers (4). Although aging is a major factor influencing TL, genetic variation also plays a key role
247 and helps explain why TL established in the zygote strongly influences TL throughout life (5).

248 Unraveling the mechanisms that determine TL in the zygote is therefore highly relevant, particularly
249 for optimizing *in vitro* fertilization strategies. A recent study in mice suggests that mitochondrial
250 dysfunction impairs telomere elongation during embryonic development-a defect that was largely
251 reversed by antioxidant treatment, highlighting the harmful effect of ROS on TL regulation in the
252 embryo (8). In humans, prenatal exposure to psychological stress has also been linked to shorter
253 leukocyte TL in offspring (27). Given the established connection between psychological and
254 oxidative stress (28,29), these findings point to a similar influence of mitochondrial function on TL

255 regulation during human embryogenesis. Building on these findings -and previous evidence
256 suggesting stronger maternal inheritance of TL in humans (6,7)- we hypothesized that the
257 mitochondrial genome may influence human TL. To investigate this, we employed a
258 transmitochondrial cybrid model using platelets from seven donors with known leukocyte TL and
259 distinct mitochondrial subhaplogroups. Notably, we observed an inverse correlation between donor
260 leukocyte TL and mitochondrial ROS levels in the cybrids, indicating that mitochondrial
261 subhaplogroup affects mitochondrial function and suggesting a potential role for mtDNA variation
262 in shaping leukocyte TL *in vivo*. Our findings further implicate CI activity in this process, as, while
263 donors #6 and #7, with signs of maternal inheritance of their long telomeres, both display
264 mitochondria with high CI activity, donor #1, with long telomeres but low mtDNA-encoded CI
265 activity, did not transmit her long telomeres to her progeny. In summary, our data indicate that low
266 levels of mitochondrial ROS, combined with potent CI activity, may be key for a mtDNA-driven
267 maternal inheritance of long telomeres. The Japanese m.C5178A longevity-associated variant in
268 the *ND2* gene (30) further supports an important role for CI in promoting mitochondrial fitness, and
269 possibly TL regulation.

270 Whether and how the centenarian-linked K1a mtDNA contributes to reduced ROS levels awaits
271 further investigation. As a defective aerobic production of ATP, linked to the ATP6 A177T variant,
272 was proposed to account for the lack of mtDNA K haplogroup in Finnish elite endurance athletes
273 (31), we hypothesize that, by reducing ATP aerobic production, ROS production decreases, thus
274 providing a possible explanation to this longevity-associated mtDNA (32). Consistent with this,
275 Cyb6 cybrids showed a distinct response to FCCP uncoupling agent as, unexpectedly, respiration
276 could not be restored in cells with oligomycin-inhibited ATP synthase, suggesting a defective ability
277 in increasing oxygen consumption rate to face an energy demand increase (Fig S4A-B). This could
278 be related to the location of the A177T variant in a crucial region of ATP6, along the proton pore
279 (33). Strikingly, 32.7% of the genetically homogeneous population of Ashkenazi Jews express the
280 ATP6 A177T variant (10). As telomeres from Ashkenazy centenarians blood cells are longer than
281 in control groups (34), it will be interesting to test the link to the m.G9055>A variant encoding ATP6
282 A177T.

283 Experimentally induced mitochondrial dysfunction leads to telomere damage (23). Mechanistically,
284 the *TTAGGG* repeats of telomeres are exquisitely sensitive to 8-oxo-guanine formation, a lesion
285 recognized by the base excision repair pathway that, after removal of the oxidized base, generates
286 single-strand breaks eventually recruiting NAD+-dependent PARP1 repair enzyme (21,35). If left
287 unrepaired in replicating cancer cells, these breaks can convert into double-strand breaks, resulting
288 in distal telomere loss and chromosomal fusions (22). In normal fibroblasts and epithelial cells,
289 telomeric 8-oxoG lesions induced by a chemoptogenetic tool were sufficient to activate p53-

290 dependent senescence (36), highlighting the harmful effects of oxidative stress at telomeres on
291 cellular function. During the generation of transmitochondrial cybrids, cells undergo a metabolic
292 shift from glycolysis to OXPHOS, accompanied by increased ROS production. Before cells adapt
293 to this shift, oxidative stress can be particularly damaging. Supporting the essential role of CI in
294 maintaining PARP1 activity *via* regulation of the NAD^+/NADH balance, mitochondrial platelets with
295 low CI activity triggered significant telomere shortening in recipient cells during early cybrid
296 formation -a loss that was prevented by co-treatment with an antioxidant and an NAD^+ precursor.
297 Although the observed telomere loss may be exacerbated by the *in vitro* oxidative stress conditions
298 -since donors with low CI activity did not show short leukocyte telomeres- our findings are
299 consistent with reports that NAD^+ supplementation can alleviate telomere dysfunction in cells from
300 dyskeratosis congenita patients (37) and improve hematopoietic function and telomere integrity in
301 $Tert^{-}/^{-}$ mice (38). Data are also consistent with the observation that mice lacking PARP display
302 telomere shortening and chromosomal instability (39). Together, these data bring support to the
303 hypothesis that, when extremely pathogenic and associated with high oxidative stress levels, such
304 as in MELAS or LHON patients (40), mutations in CI may impair telomere length resetting *in utero*.

305 Our study also unexpectedly revealed a reduction in telomere length in 143B cells following
306 mitochondrial depletion. This telomere shortening was associated with decreased telomerase
307 activity, as measured by ddTRAP, but not with reduced expression of the telomerase subunits
308 h*TERT* or h*TR*. 143B osteosarcoma cells are deficient in thymidine kinase 1 and therefore lack an
309 effective pyrimidine salvage pathway. In the absence of oxidative phosphorylation, the *de novo*
310 thymidine synthesis pathway is also compromised, rendering 143B ρ^0 cells dependent on uridine
311 supplementation for survival. Although this hypothesis requires further investigation, we propose
312 that the shorter telomeres observed in 143B ρ^0 cells may be linked to the emerging role of thymidine
313 nucleotide metabolism in the regulation of human telomere length, potentially through an allosteric
314 effect of dTTP on telomerase activity (41-43).
315

316 Altogether, our findings that certain mitochondrial genomes may support telomere elongation are
317 relevant to three-parent *in vitro* fertilization, a technique that uses donor eggs to prevent the
318 transmission of mitochondrial diseases from mother to child (44). Future work will be necessary to
319 investigate how mitochondrial activity may be involved and whether the nucleotide metabolism that
320 recently emerged as an important regulator of telomerase activity may play additional role.

321
322
323 **Materials and Methods**

324

325 **Human study participants**

326 Blood samples were obtained from a total of 491 healthy donors. Cohort characteristics are as
327 follows: 261 females and 230 males, median age of 26.3 y (7 days-99.2 y). Protocols were
328 approved by the CHEF institutional Ethics committee and written informed consents were obtained
329 from all 18 year-old or over volunteers. For children below 18, left-over blood samples were
330 obtained through the Cliniques universitaires Saint-Luc after screening for inclusion.

331 **Leukocyte purification**

332 Blood samples were collected in EDTA tubes and kept at room temperature for a maximum of 48
333 h before processing. Leukocytes were purified after erythrocyte lysis with ice-cold 0.155 M NH_4Cl
334 (Sigma-Aldrich), 0.01 M $KHCO_3$ (Sigma-Aldrich) and 0.1 mM EDTA (Sigma-Aldrich) solution as
335 described (12). Leukocytes were then resuspended in hybridization buffer (5 % dextrose/10 mM
336 HEPES/0.1 % BSA), and frozen at -80 °C in 80 % FBS (Cytiva)/20 % DMSO (Sigma-Aldrich).

337 **Flow-FISH**

338 The average telomere length (TL) was measured in peripheral blood leucocytes by flow cytometry
339 combined with FISH (Flow-FISH), using bovine thymocytes as reference as previously described
340 (12). TL of bovine thymocytes was measured by telomere restriction fragment (TRF) analysis (see
341 below). TL was evaluated in lymphocyte and granulocyte populations distinguished by LDS751
342 staining of DNA as described (12). The telomeric PNA probe was as follows: FITC-OO-
343 CCCTAACCCTAACCCTAA (Panagene). Values obtained for TL in lymphocytes and granulocytes
344 are provided in Table S1.

345 **Genomic DNA extraction**

346 Genomic DNA was extracted by overnight digestion at 45°C with 100 μg/mL proteinase K (Sigma-
347 Aldrich) in lysis buffer (10 mM Tris–HCl, 10 mM EDTA, 1 % SDS; pH 8.0) followed by DNA
348 purification with 25:24:1 phenol–chloroform–isoamyl alcohol (Sigma-Aldrich) and precipitation in
349 isopropanol (Thermo Fisher Scientific) and 0.3 M sodium acetate; pH 5.5 (Sigma-Aldrich). gDNA
350 was subsequently treated with 0.2 mg/mL RNAse A (Thermo Fisher Scientific) for 1 h at 37 °C,
351 purified, and precipitated again as described above. DNA concentration, purity and integrity were
352 evaluated with Nanodrop (Thermo Fisher Scientific).

353 **MtDNA subhaplogroup identification**

354 PCR reactions were performed on 20-50 ng total DNA using GoTaq® G2 DNA Polymerase
355 (Promega) and the primers provided in Table S2 so as to cover the entire mtDNA sequence (45).
356 PCR program was as follows: 3 min at 95 °C followed by 40 cycles of 95 °C for 45 s, 47/50/55 °C
357 for 45 s, and 72 °C for 1 min, with a final step at 72 °C for 5 min. PCR products were loaded on 1
358 % agarose gel (Eurogentec), stained with 0.5 μg/mL ethidium bromide (Sigma-Aldrich) and
359 extracted from the gel using SmartPure Gel Kit (Eurogentec), according to the manufacturer's
360 instructions, followed by Sanger sequencing (Azenta/Genewiz). MtDNA subhaplogroups were
361 identified using MITOMASTER tool on mitomap.org website.

362 **MtDNA content quantification**

363 MtDNA content quantification was performed by qPCR on 60 ng of total DNA, using KAPA SYBR
364 FAST (Sigma-Aldrich) and primer sequences (45) provided in Table S2.

365 **Cell culture and treatments**

366 143B cells and cybrids were grown in DMEM high glucose (4.5 g/L) supplemented with 10 % FBS
367 (Cytiva) and 1 % Penicillin/Streptomycin (Capricorn Scientific). 143B ρ^0 cells were grown in DMEM
368 high glucose supplemented with 0.11 g/L pyruvate (Thermo Fisher Scientific), 10 % FBS (Cytiva),
369 50 μg/mL uridine (Sigma-Aldrich) and 1 % Penicillin/Streptomycin (Capricorn Scientific). For the
370 subcloning of 143B ρ^0 population, cells were treated exactly as if they would undergo fusion with
371 platelets and kept throughout the cloning process in ρ^0culture medium. All cell lines were regularly
372 checked for mycoplasma contamination. For this, 100 µL of culture medium were heated at 95°C
373 for 5 min before spinning down. qPCR reactions were performed on 2 µL of the supernatant as
374 described previously (46) using primers listed in Table S2.

375 **Isolation of human platelets**

376 Blood was collected in 8.5 mL-CPDA tubes (Sarstedt) and centrifuged at 330 x *g* for 20 min at 22
377 °C. The upper platelet-rich plasma fraction was treated with 4 µg/mL eptifibatide (GlaxoSmithKline)
378 and 1 U/mL apyrase (Sigma-Aldrich) on ice before centrifugation at 800 x *g* for 10 min at room
379 temperature. The pellet was resuspended into 5 mL physiological saline solution containing 4
380 µg/mL eptifibatide and 1 U/mL apyrase. Platelets were counted and diluted with the saline solution
381 to obtain 10^5 platelets/µL and stored for 30-45 min at 37 °C. 40 x 10^6 platelets were then transferred
382 into a 2 mL Eppendorf tube, centrifuged at 800 x *g* for 10 min at room temperature and directly
383 processed for fusion with 143B ρ^0 cells.

384 **Cybrid formation**

385 Cybrids were obtained as previously described (19). A detailed protocol is provided as
386 Supplementary information.

387 **Generation of new 143B ρ^0 clones**

388 New 143B ρ^0 clones were generated as previously described (47). Briefly, 1×10^5 cells were seeded
389 in 10-cm dishes and allowed to adhere overnight at 37 °C. Cells were then cultured in DMEM, High
390 Glucose, Pyruvate (Gibco, 41966029) supplemented with 10% FBS, 1% penicillin–streptomycin,
391 50 µg/ml freshly added uridine (Sigma, U3003), and 50 ng/ml ethidium bromide (Invitrogen,
392 15585011). The treatment was maintained for 4 weeks prior to clonal isolation. MtDNA depletion
393 in the resulting clones was checked by qPCR as described above.

394 **Mitochondrial superoxide assessment by EPR spectroscopy**

395 The electron paramagnetic resonance (EPR) assay is based on the oxidation of Mito-TEMPO-H, a
396 diamagnetic cyclic hydroxylamine that accumulates inside the mitochondria and is transformed into
397 a paramagnetic nitroxide. To isolate the contribution of superoxide to the oxidation of the probe,
398 PEG-SOD2 was used as a control as described previously (24,48-50). A detailed protocol is
399 provided as Supplementary information.

400 **Seahorse analyses**

401 Oxygen consumption rates (OCR) were measured using a Seahorse XFe96 plate reader (Agilent).
402 All assays were carried out using a seeding density of 10,000 cells/well in non-buffered DMEM,
403 adjusted at pH 7.4. Mitochondrial function parameters (*i.e.* basal and maximal respirations and ATP
404 production-linked OCR) were evaluated, with the XF Cell MitoStress Test (Agilent), after sequential
405 treatment with 1 µM oligomycin, 1 µM FCCP and 0.5 µM rotenone/antimycin A, as previously
406 described (51). ETC complex activity was assessed as previously reported (52), with slight
407 modifications. Briefly, 10^4 cells per well were first permeabilized with 1 nM Seahorse XF Plasma
408 Membrane Permeabilizer (Agilent) and respiration was stimulated by adding 10 mM pyruvate, 5
409 mM malate, and 2 mM ADP. After the baseline scan, 100 nM rotenone was then added to inhibit
410 complex I and 10 mM succinate was injected to establish complex II respiration. Last, 4 µM
411 antimycin A was added to inhibit complex III and 100 µM N,N,N',N'-Tetramethyl-p-
412 phenylenediamine dihydrochloride (TMPD) + 10 mM ascorbate was injected as a complex IV
413 substrate. OCR data were then normalized according to protein content in each experimental well.

414 **Telomere restriction fragment (TRF) length analysis**

415 TRF analyses were performed as described previously (53) on 2-5 µg of RNAse-treated genomic
416 DNA digested with 20 U *Hinf*I and 20 U *Rsa*I and using [γ-^{32}P] ATP-labelled $(TAACCC)_4$ probe.

417 Smart Ladder (Eurogentec) was run together with the samples, stained with ethidium bromide and
418 imaged with a ruler. TRF were quantified using the online available WALTER (Web-based Analyser
419 of the Length of Telomeres) software (https://www.ceitec.eu/chromatin-molecular-
420 complexes/rg51/tab?tabId=125#WALTER).

421 **TeSLA analysis**

422 The procedure described previously (54) was followed for TeSLA analysis. Primer sequences are
423 provided in Table S2.

424 **Immunofluorescence and fluorescence *in situ* hybridization**

425 Immunofluorescence and FISH experiments were performed as described previously (53) using
426 the following antibodies and telomeric probe: rabbit anti-53BP1 (Novus Biologicals), Alexa 488 goat
427 anti-rabbit (Invitrogen), mouse anti-Poly(ADP-ribose) (Millipore), Alexa 488 Goat anti-mouse
428 (Abcam), 5'(TYE 563)GGGTtAGGGttAGgGTTAGGGttAGGGttAGGGtTA(TYE 563) (small letters
429 indicate LNA™ modified bases) (Qiagen). For the detection of parylated proteins, cells were grown
430 in the presence of 1 μM PDD00017273 PARG inhibitor (Sigma-Aldrich). For telomeric FISH on
431 metaphase spreads, cells were treated as described previously (55) and telomeres were probed
432 with 5'(TYE 563)GGGTtAGGGttAGgGTTAGGGttAGGGttAGGGtTA(TYE 563). Images were
433 acquired with the Cell Observer Spinning Disk confocal microscope (Zeiss) with 100× objective and
434 analyzed using ImageJ software (National Institute of Health), while maintaining the same threshold
435 for samples from the same experiment.

436 **Liquid chromatography-mass spectrometry analysis of metabolites**

437 6-well plates with cultured cells were rapidly washed twice with ice cold water and submerged in
438 liquid nitrogen. 300 μL of a solution of 90 % methanol and 10 % chloroform were added, lysates
439 were scraped and transferred to microcentrifuge tubes for centrifugation for 15 min at 4 °C and 22,
440 000 x *g*. The supernatants were dried in a Speed-Vac vacuum concentrating system and
441 resuspended into 50 μL of 50:50 water:methanol solution. Analyses by LC-MS were performed as
442 previously described (56) based on a method by Coulier *et al.* (57). A detailed protocol is provided
443 as Supplementary information.

444 **Dosage of extracellular glucose and lactate**

445 Glucose and lactate concentrations were measured in extracellular media by using specific
446 enzymatic assays and an ISCUSflex microdialysis analyzer (M Dialysis), as previously described
447 (51).

448 **RNA isolation and reverse transcription quantitative real-time PCR**

449 RNA was extracted using TriPure Isolation Reagent (Sigma-Aldrich) according to the
450 manufacturer's instructions. For cDNA synthesis, 1 µg of RNA was retro-transcribed with 200 U
451 MMLV-RT (Thermo Fisher Scientific), 0.2 µg random hexamers (Thermo Fisher Scientific), 20 U
452 RiboLock RNase inhibitor (Thermo Fisher Scientific) and 2 mM dNTP mix. qPCR reactions were
453 performed using KAPA SYBR FAST (Sigma-Aldrich) and the following program: 95°C for 10 min
454 followed by 40 cycles of 95 °C for 15 sec and 60 °C for 30 sec.
455 Primer sequences are provided in Table S2.

456 **Telomerase repeat amplification protocol (TRAP) and droplet digital TRAP (ddTRAP)**

457 For telomerase activity assessment *in vitro* using the TRAP assay, 500,000 cells were lysed in
458 100 µL CHAPS lysis buffer (TRAPeze S7700, Millipore) on ice for 30 min and proteins were
459 quantified by Bradford assay (Bio-Rad). 500 ng of the lysis mixture were subjected to the TRAP
460 assay following the Millipore kit instructions and TRAP products were separated on
461 TBE/acrylamide:bisacrylamide (19:1) gel and visualized by staining with SYBR Gold Nucleic Acid
462 GelStain (Invitrogen) with a PhosphoImager (Fujitsu). For ddTRAP (58), 500 ng of the lysis mixture
463 were added to 50 µL of 1× TRAP buffer (200 mM Tris–HCl, pH 8.3, 15 mM $MgCl_2$, 2.5 mM each
464 dNTPs, 200 mM TS primer (Table S2), and 0.4 mg/ml BSA), and extension reaction was performed
465 by incubating the mix at 25°C for 40 min, followed by deactivation at 95°C for 5 min. For the ddPCR
466 reaction, 3.75 µL of lysis-extension mix were added to 1x EvaGreen QX200 Super-mix (Bio-Rad),
467 50 nM TS primer, 50 nM ACX primer (Table S2) and H_20 up to 25 µL. PCR reaction was performed
468 as follows: initial denaturation for 5 min at 95°C followed by 40 cycles of 95°C/30 s, 54°C/30 s, and
469 72°C/30 s. Data were analyzed on Quantasoft software.

470 **Statistics**

471 Statistical analyses were performed using PRISM 8 software. Normality of the data was always
472 checked before statistical tests. Details are provided in the Figure legends. Nomograms for Flow-
473 FISH-based measurements of TL in the healthy population were drawn using the Age-related
474 reference interval function of MedCalc Software (Belgium) based on methods described previously
475 (59-61).

476 **Acknowledgments**
477
478 We are grateful to all volunteers for providing blood samples. We thank Sandrine Horman, Marie
479 Octave and Valentine Robaux for help with platelet purification and Géraldine Aubert and Mary
480 Armanios for guidance in Flow-FISH. We are grateful to Victoria Van Regemorter and Caroline
481 Huart for sharing unpublished data on TL in their cohort. We thank Chloé Despontin and Antoine

Fattaccioli for technical support, Céline Coquette for help with blood collection and Mélina Vaurs, and Nausica Arnoult for critical reading of the manuscript. This work was supported by the Fonds National pour la Recherche Scientifique (FNRS) (Belgium), The Belgian Foundation against Cancer and WELBIO (Walloon Excellence in Life Sciences and Biotechnology) (grant X250624 to CC). Patrick Revy's team is Labellisé Ligue (France). We are grateful to the de Duve Institute for constant support.

References

1. T. de Lange, Shelterin-Mediated Telomere Protection. *Annu. Rev. Genet.* 52, 223-247(2018).
2. J. Campisi, J. K. Andersen, P. Kapahi, S. Melov, Cellular senescence: a link between cancer and age-related degenerative disease? *Semin. Cancer Biol.* 21, 354-359 (2011)
3. C. López-Otín, M.A. Blasco, L. Partridge, M. Serrano, G. Kroemer, Hallmarks of aging: an expanding universe. *Cell* 186, 243-278 (2023)
4. C.V. Schneider *et al*., Association of telomere length with risk of disease and mortality. *JAMA Intern. Med.* 182, 291-300 (2022)
5. K. Demanelis *et al*., Determinants of telomere length across human tissues. *Science* 369:eaaz6876 (2020)
6. L. Broer *et al*., Meta-analysis of telomere length in 19,713 subjects reveals high heritability, stronger maternal inheritance and a paternal age effect. *Eur. J. Hum. Genet.* 21, 1163-1168 (2013)
7. S. Schaetzlein *et al.*, Telomere length is reset during early mammalian embryogenesis. *Proc. Natl. Acad. Sci. U. S. A.* 101, 8034-8038 (2004)
8. Y.E. Winstanley *et al.*, Telomere length in offspring is determined by mitochondrial-nuclear communication at fertilization. *Nat. Commun.* 16, 2527 (2025)
9. K. Oexle, A. Zwirner, Advanced telomere shortening in respiratory chain disorders. *Hum. Mol. Genet.* 6, 905-908 (1997)
10. E. Ruiz-Pesini *et al.*, An enhanced MITOMAP with a global mtDNA mutational phylogeny. *Nucleic Acids Res.* 35, D823-828 (2007)
11. L. Nersisyan, M. Nikoghosyan, Genome of the Netherlands consortium, A. Arakelyan, WGS-based telomere length analysis in Dutch family trios implicates stronger maternal inheritance and a role for RRM1 gene. *Sci. Rep.* 9, 18758 (2019)
12. G.M. Baerlocher, I. Vulto, G. de Jong, P.M. Lansdorp, Flow cytometry and FISH to measure the average length of telomeres (flow FISH). *Nat. Protoc.* 1, 2365-2376 (2006)
13. J.K. Alder *et al.,* Short telomeres are a risk factor for idiopathic pulmonary fibrosis. *Proc. Natl. Acad. Sci. U. S. A.* 105, 13051-13056 (2008)
14. G. Aubert, G. M. Baerlocher, I. Vulto, S. S. Poon, P.M. Lansdorp, Collapse of telomere homeostasis in hematopoietic cells caused by heterozygous mutations in telomerase genes. *PLoS Genet.* 8, e1002696 (2012)
15. E. Mundstock *et al.*, Effect of obesity on telomere length: Systematic review and meta-analysis. *Obesity (Silver Spring)* 23, 2165-2174 (2015)
16. M. Asghar, S. Bensch, M. Tarka, B. Hansson, D. Hasselquist, Maternal and genetic factors determine early life telomere length. *Proc. Biol. Sci.* 282, 20142263 (2015)

525 17. R. Ivanova, V. Lepage, D. Charron, F. Schachter, Mitochondrial genotype associated with
526 French Caucasian centenarians. *Gerontology* 44, 349 (1998)
527 18. O.A. Ross *et al*., Mitochondrial DNA polymorphism: its role in longevity of the Irish
528 population. *Exp. Gerontol.* 36, 1161-1178 (2001)
529 19. M.P. King, G. Attardi, Human cells lacking mtDNA: repopulation with exogenous
530 mitochondria by complementation. *Science* 246, 500-503 (1989)
531 20. P. Belenky, K. L. Bogan, C. Brenner, NAD+ metabolism in health and disease. *Trends*
532 *Biochem. Sci.* 32, 12-19 (2007)
533 21. R.P. Barnes, E. Fouquerel, P.L. Opresko, The impact of oxidative DNA damage and stress
534 on telomere homeostasis. *Mech. Ageing Dev.* 177, 37-45 (2019)
535 22. E. Fouquerel *et al.*, Targeted and Persistent 8-Oxoguanine Base Damage at Telomeres
536 Promotes Telomere Loss and Crisis. *Mol. Cell* 75, 117-130 (2019)
537 23. W. Qian *et al.*, Chemoptogenetic damage to mitochondria causes rapid telomere
538 dysfunction. *Proc. Natl. Acad. Sci. U. S. A.* 116, 18435-18444 (2019)
539 24. D. d'Hose *et al.*, A versatile EPR toolbox for the simultaneous measurement of oxygen
540 consumption and superoxide production. *Redox Biol.* 40, 101852 (2021)
541 25. V. Castaneda, A. Haro-Vinueza, I. Salinas, A. Caicedo, M.A. Mendez, The MitoAging
542 Project: Single nucleotide polymorphisms (SNPs) in mitochondrial genes and their
543 association to longevity. *Mitochondrion* 66, 13-26 (2022)
544 26. A. Froidure *et al.*, Short telomeres increase the risk of severe COVID-19. *Aging (Albany*
545 *NY)* 12, 19911-19922 (2020)
546 27. S. Entringer *et al.*, Stress exposure in intrauterine life is associated with shorter telomere
547 length in young adulthood. *Proc. Natl. Acad. Sci. U.S.A.* 108, E513-518 (2011)
548 28. S. Salim, Oxidative stress and psychological disorders. *Curr Neurophrmacol* 12, 140-147
549 (2014)
550 29. R. Rzasa *et al.*, Association of acute psychological stress with oxidative stress: evidence
551 from serum analysis. *Redox Biol.* 47, 102138 (2021)
552 30. M. Tanaka, J.S. Gong, J. Zhang, M. Yoneda, K. Yagi, Mitochondrial genotype associated
553 with longevity. *Lancet* 351, 185-186 (1998)
554 31. A.K. Niemi, K. Majamaa, Mitochondrial DNA and ACTN3 genotypes in Finnish elite
555 endurance and sprint athletes. *Eur. J. Hum. Genet.* 13, 965-969 (2005)
556 32. N. Eynon, M. Moran, R. Birk, A. Lucia, The champions' mitochondria: is it genetically
557 determined? A review on mitochondrial DNA and elite athletic performance. *Physiol.*
558 *Genomics* 43, 789-798 (2011)
559 33. R.D. Ganetzky *et al.*, MT-ATP6 mitochondrial disease variants: Phenotypic and
560 biochemical features analysis in 218 published cases and cohort of 14 new cases. *Hum.*
561 *Mutat.* 40, 499-515 (2019)
562 34. G. Atzmon *et al.*, Genetic variation in human telomerase is associated with telomere length
563 in Ashkenazi centenarians. *Proc. Natl. Acad. Sci. U. S. A.* 107 Suppl 1, 1710-1717 (2010)
564 35. J.F. Passos, G. Saretzki, T. von Zglinicki, DNA damage in telomeres and mitochondria
565 during cellular senescence: is there a connection? *Nucleic Acids Res.* 35, 7505-7513
566 (2007)
567 36. R.P. Barnes *et al.*, Telomeric 8-oxo-guanine drives rapid premature senescence in the
568 absence of telomere shortening. *Nat. Struct. Mol. Biol.* 29, 639-652 (2022)
569 37. C. Sun *et al.*, Re-equilibration of imbalanced NAD metabolism ameliorates the impact of
570 telomere dysfunction. *EMBO J.* 39, e103420 (2020)

571 38. A.J. Stock *et al.*, Boosting NAD ameliorates hematopoietic impairment linked to short
572 telomeres in vivo. *Geroscience* 45, 2213-2228 (2023)
573 39. F. d'Adda di Fagagna *et al.*, Functions of poly(ADP-ribose) polymerase in controlling
574 telomere length and chromosomal stability. *Nat. Genet.* 23, 76-80 (1999)
575 40. Y. Zhuo, H. Luo, K. Zhang, Leber hereditary optic neuropathy and oxidative stress. *Proc.*
576 *Natl. Acad. Sci. U. S. A.* 109, 19882-19883 (2012)
577 41. C. Li *et al.*, Genome-wide association analysis in humans links nucleotide metabolism to
578 leukocyte telomere length. *Am. J. Hum. Genet.* 106, 389-404 (2020)
579 42. H. Tummala *et al.*, Germline thymidylate synthase deficiency impacts nucleotide
580 metabolism and causes dyskeratosis congenita. *Am. J. Hum. Genet.* 109, 1472-1483
581 (2022)
582 43. W. Mannherz, S. Agarwal, Thymidine nucleotide metabolism controls human telomere
583 length. *Nat. Genet.* 55, 568-580 (2023)
584 44. E. Callaway, First UK children born using three-person IVF: what scientists want to know.
585 *Nature* 617, 443-444 (2023)
586 45. C.U. Huebbers *et al.*, High glucose uptake unexpectedly is accompanied by high levels of
587 the mitochondrial ss-F1-ATPase subunit in head and neck squamous cell carcinoma.
588 *Oncotarget* 6, 36172-36184 (2015)
589 46. L. Dreolini *et al.*, A rapid and sensitive nucleic acid amplification technique for mycoplasma
590 screening of cell therapy products. *Mol. Ther. Methods Clin. Dev.* 17, 393-399 (2020)
591 47. M.P. King, G. Attardi, Isolation of human cell lines lacking mitochondrial DNA. *Methods*
592 *Enzymol.* 264, 304-313 (1996)
593 48. S. Scheinok, T. Capeloa, P.E. Porporato, P. Sonveaux,, B. Gallez, An EPR study using
594 cyclic hydroxylamines to assess the level of mitochondrial ROS in superinvasive cancer
595 cells. *Cell. Biochem. Biophys.* 78, 249-254 (2020)
596 49. S.I. Dikalov, I.A. Kirilyuk, M. Voinov, I.A. Grigor'ev, EPR detection of cellular and
597 mitochondrial superoxide using cyclic hydroxylamines. *Free Radic. Res.* 45, 417-430
598 (2011)
599 50. S.I. Dikalov, D.G. Harrison, Methods for detection of mitochondrial and cellular reactive
600 oxygen species. *Antioxid. Redox Signal.* 20, 372-382 (2014)
601 51. C. Vander Linden *et al.*, Therapy-induced DNA methylation inactivates MCT1 and renders
602 tumor cells vulnerable to MCT4 inhibition. *Cell Rep.* 35, 109202 (2021)
603 52. F. Virga *et al.*, Macrophage miR-210 induction and metabolic reprogramming in response
604 to pathogen interaction boost life-threatening inflammation. *Sci. Adv.* 7, eabf0466 (2021)
605 53. H. Episkopou, A. Diman, E. Claude, N. Viceconte, A. Decottignies, TSPYL5 depletion
606 induces specific death of ALT cells through USP7-dependent proteasomal degradation of
607 POT1. *Mol. Cell* 75, 469-482 (2019)
608 54. T.P. Lai *et al.*, A method for measuring the distribution of the shortest telomeres in cells and
609 tissues. *Nat. Commun.* 8, 1356 (2017)
610 55. N. Viceconte *et al.,* Highly aggressive metastatic melanoma cells unable to maintain
611 telomere length. *Cell Rep.* 19, 2529-2543 (2017)
612 56. I.P. Heremans *et al.*, Parkinson's disease protein PARK7 prevents metabolite and protein
613 damage caused by a glycolytic metabolite. *Proc. Natl. Acad. Sci. U. S. A.* 119, e2111338119
614 (2022)

615 57. L. Coulier *et al.*, Simultaneous quantitative analysis of metabolites using ion-pair liquid
616 chromatography-electrospray ionization mass spectrometry. *Anal. Chem.* 78, 6573-6582
617 (2006)
618 58. A.T. Ludlow, D. Shelton, W.E. Wright, J.W. Shay, ddTRAP: a method for sensitive and
619 precise quantification of telomerase activity. *Methods Mol. Biol.* 1768, 513-529 (2018)
620 59. E.M. Wright, P. Royston, Simplified estimation of age-specific reference intervals for
621 skewed data. *Stat. Med.* 16, 2785-2803 (1997)
622 60. D.G. Altman, Construction of age-related reference centiles using absolute residuals. *Stat.*
623 *Med.* 12, 917-924 (1993)
624 61. D.G. Altman, L.S. Chitty, Design and analysis of studies to derive charts of fetal size.
625 *Ultrasound Obstet. Gynecol.* 3, 378-384 (1993)

Figures and Tables

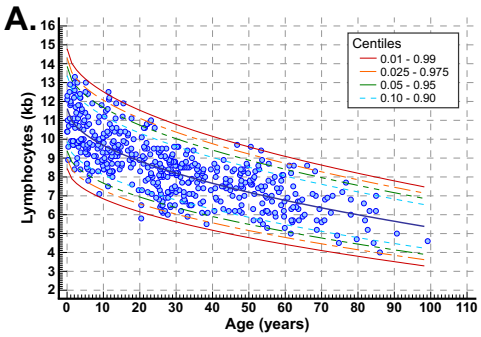

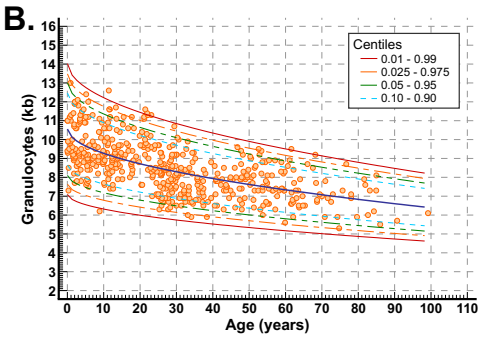

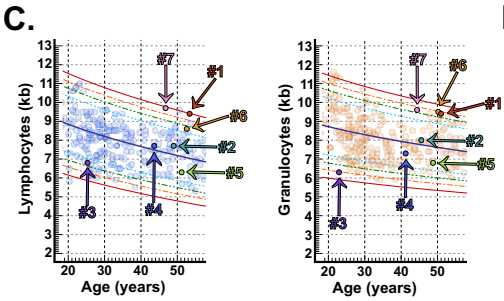

D.

Donor	Subhaplogroup	Rare variant (complex)	Variant frequency	
			Overall	In subhaplogroup
#1	T2b4a	ND2 N150D (CI)	5.8%	100%
#2	H56b	/	/	/
#3	H	COX1 F63L (CIV)	0.002%	0%
		ATP8 M16L (CV)	0.004%	0.2%
#4	H6a1a	ND4 S418P (CI)	0.06%	0%
		ND4 I165T (CI)	0.7%	51.8%
#5	H2a2a1	/	/	/
#6	K1a4a1	ATP6 A177T (CV)	5.4%	99%
		COB F18L (CIII)	8.8%	99.6%
#7	H1b1e	ND1 T164A (CI)	0.8%	29.5%

630

631 **Figure 1. Establishment of Flow-FISH reference curves for telomere length A.** The age-related
632 reference interval and centiles were calculated after telomere length measurement by Flow-FISH
633 in lymphocytes obtained from 491 healthy donors. The P50 curve is shown in dark blue. Other
634 percentile curves are shown as indicated in the legend. **B.** Same as A in granulocytes. **C.** TL in
635 lymphocytes (left) or granulocytes (right) of eight selected donors. **D.** Mitochondrial subhaplogroups
636 of the eight selected donors with an overview of the variants showing both a change in the amino
637 acid sequence and an overall frequency of less than 10% in Mitomap database in the mtDNA
638 coding regions of the donors. The variant frequency in the subhaplogroup of each donor is indicated
639 in the last column.

640

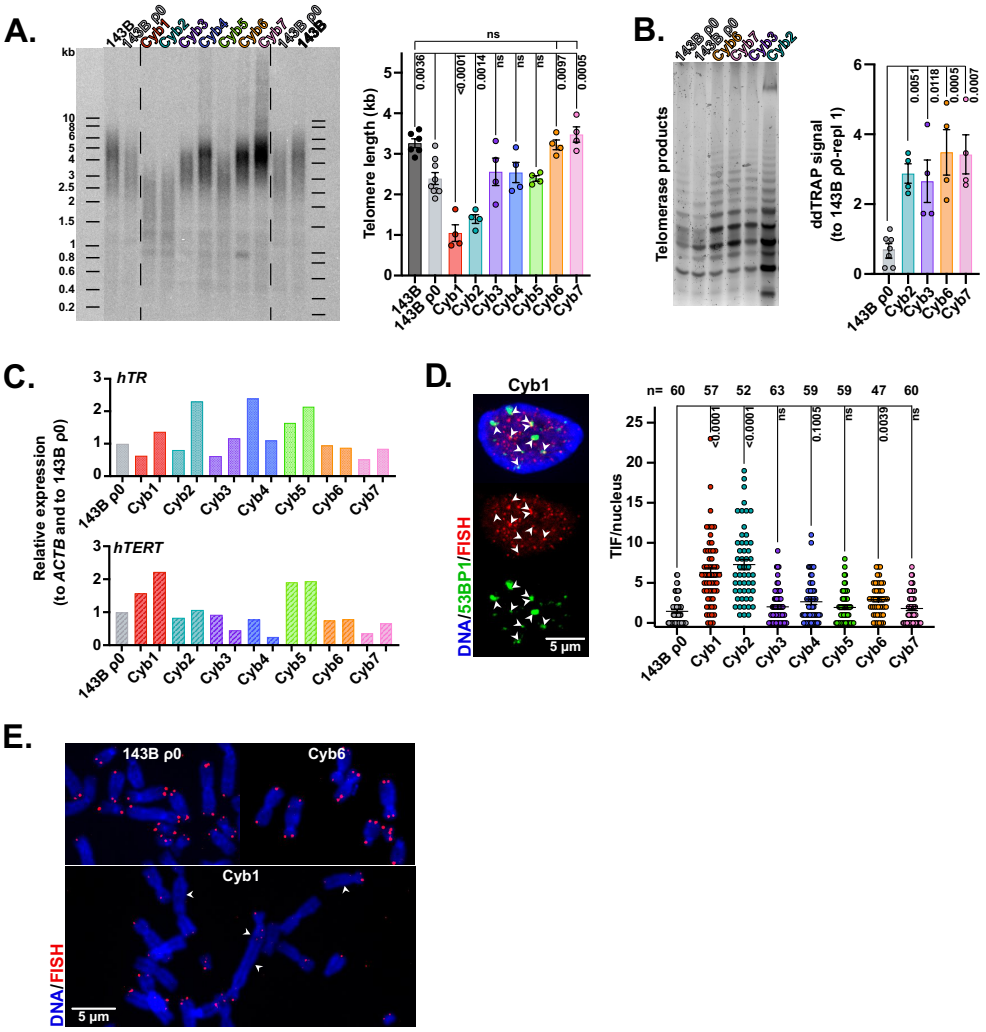
A.
143B
143B p0
Cyb1
Cyb2
Cyb3
Cyb4
Cyb5
Cyb6
Cyb7
kb
Telomere length (kb)
ns
0.0036
<0.0001
0.0014
ns
ns
ns
0.0097
0.0005
B.
Telomerase products
ddTRAP signal
(to 143B p0-repl 1)
0.0051
0.0118
0.0015
0.0007
C.
hTR
hTERT
Relative expression
(to ACTB and to 143B p0)
D.
Cyb1
DNA/53BP1/FISH
5 µm
n= 60 57 52 63 59 59 47 60
TIF/nucleus
<0.0001
<0.0001
ns
0.1005
ns
0.0039
ns
E.
143B p0
Cyb6
Cyb1
DNA/FISH
5 µm

641

642
643
644 **Figure 2. Mitochondrial genomes modulate telomere length and integrity of ρ^0 recipient cells.**
645 **A.** Left: Representative Southern blot analysis (TRF) of telomeres in 143B, 143B ρ^0 recipient cells
646 and in one cybrid clone from each donor at the first PDs post-selection. Right: Quantification of
647 TRF on four independent cybrid clones for each. Mean ± SEM. One-way ANOVA. ns: p>0.05. **B.**
648 Left: TRAP assay products for the indicated cell lines. Right: ddTRAP quantification of telomerase
649 activity in the indicated cell lines. Copy number concentrations were normalized to the first replicate
650 of 143B ρ^0 cells (repl 1). Mean ± SEM. One-way ANOVA. **C.** qRT-PCR analysis of h*TR* and h*TERT*
651 transcripts. Values were normalized first to *ACTB* mRNA levels and then to 143B ρ^0 ratio. **D.** Left:
652 Representative pictures of telomere dysfunction-induced foci (TIF) detection by co-localization of
653 telomeres (red FISH probe) with 53BP1 DNA damage marker (green). White arrowheads indicate
654 TIF. Blue: DAPI. Scale bar: 5 μm. Right: TIF quantification in clone #1 of all cybrids (first PDs post-
655 selection) and in 143B ρ^0 cells. n=47-63 nuclei. Mean ± SEM. Kruskal-Wallis test. ns: p>0.05. **E.**
656 Visualisation of telomere fusions (white arrowheads) in Cyb1 cells at PD7. 143B ρ^0 and Cyb6 cells
657 are shown as controls. Telomeres are detected by FISH (red) and DAPI stains DNA (blue). Scale
658 bar: 5 μm.
659
660

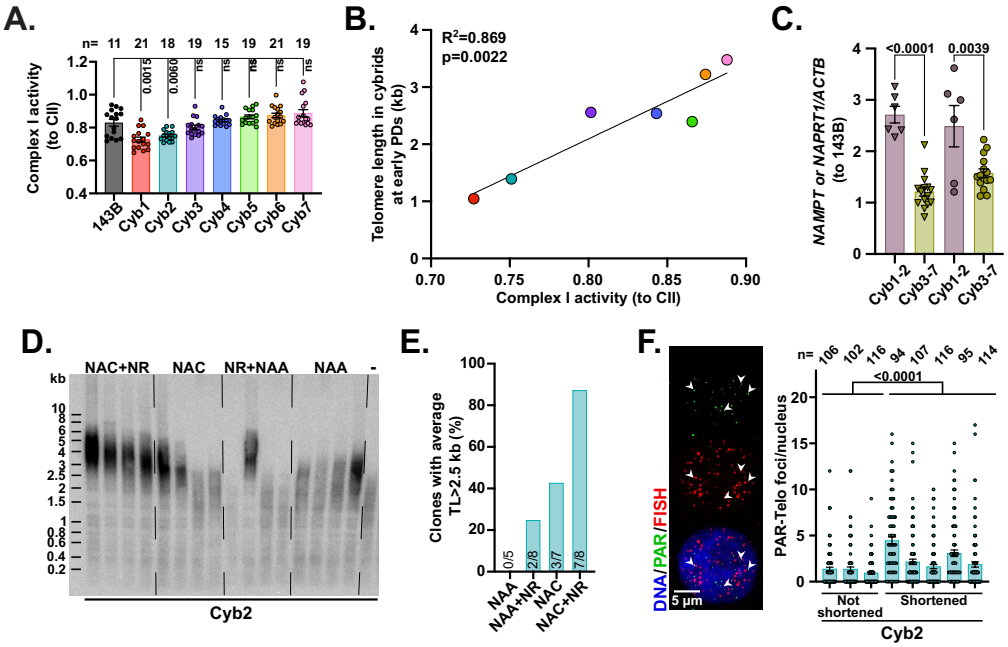
A.
n= 11 21 18 19 15 19 21 19
Complex I activity (to CII)
0.0015
0.0060
ns
143B
Cyb1
Cyb2
Cyb3
Cyb4
Cyb5
Cyb6
Cyb7
B.
R²=0.869
p=0.0022
Telomere length in cybrids at early PDs (kb)
Complex I activity (to CII)
C.
<0.0001
0.0039
NAMPT or NAPRT1/ACTB (to 143B)
Cyb1-2
Cyb3-7
Cyb1-2
Cyb3-7
D.
NAC+NR
NAC
NR+NAA
NAA
-
kb
Cyb2
E.
Clones with average TL>2.5 kb (%)
0/5
2/8
3/7
7/8
NAA
NAA+NR
NAC
NAC+NR
F.
DNA/PAR/FISH
5 µm
n= 106 102 116 94 107 116 95 114
<0.0001
PAR-Telo foci/nucleus
Not shortened
Shortened
Cyb2

661

662 **Figure 3. Telomere shortening in cybrids from donor with low complex I activity is**
663 **counteracted by antioxidant and NAD^+ precursor. A.** Complex I (CI) activity in 143B and in the
664 cybrids. Values were normalized to the activity of complex II (CII) which is entirely nuclear-encoded.
665 n measurements from 2 biological replicates on clone #1 from all: at PD 4-7 or PD 16-24 post-
666 selection. Mean ± SEM. Kruskal-Wallis test. ns: $p>0.05$. **B.** Correlation between TL in the cybrids
667 at early PDs and average ratios of CI/CII activity. Color code as in A. **C.** Expression of *NAMPT* and
668 *NAPRT1* genes from the NAD^+ salvage pathway in cybrids (PD≥5 post-selection) from donors with
669 either low (Cyb1 to 2) or normal (Cyb3 to 7) CI activity. Values were normalized to *ACTB* and to
670 the ratios measured in 143B cells. Color code as in A. n=3 biological replicates. Mean ± SEM. Two-
671 tailed Student's *t* tests. **D.** Representative TRF analysis of TL in cybrids obtained by fusion between
672 donor #2's platelets and 143B ρ^0 recipient cells in the presence of the indicated treatments or in
673 the absence of added drug (-). 5 mM N-acetyl-L-cysteine (NAC), 5 mM N-acetyl-L-alanine (NAA,
674 control) and/or 3 mM nicotinamide riboside (NR) were added at the time of the fusion and kept until
675 clone isolation. **E.** TL was measured in the following numbers of independent clones: 5 (NAA), 7
676 (NAC), 8 (NAC + NR or NAA + NR) and the percentage of clones with average TL>2.5 kb was
677 calculated. **F.** Representative images and quantification of telomeric parylation in Cyb2 cells
678 comparing cells that did or did not exhibit telomere shortening during the initial PDs following
679 cybridisation (from panel D-E). Parylation was detected by IF (green) in the presence or PARG
680 inhibitor; telomeres were detected by FISH (red) and DNA was stained with DAPI (blue). Scale bar:
681 5 μm. n=94-116 nuclei were counted for each clone. Mean ± SEM. Two-tailed Mann-Whitney test.

682
683
684

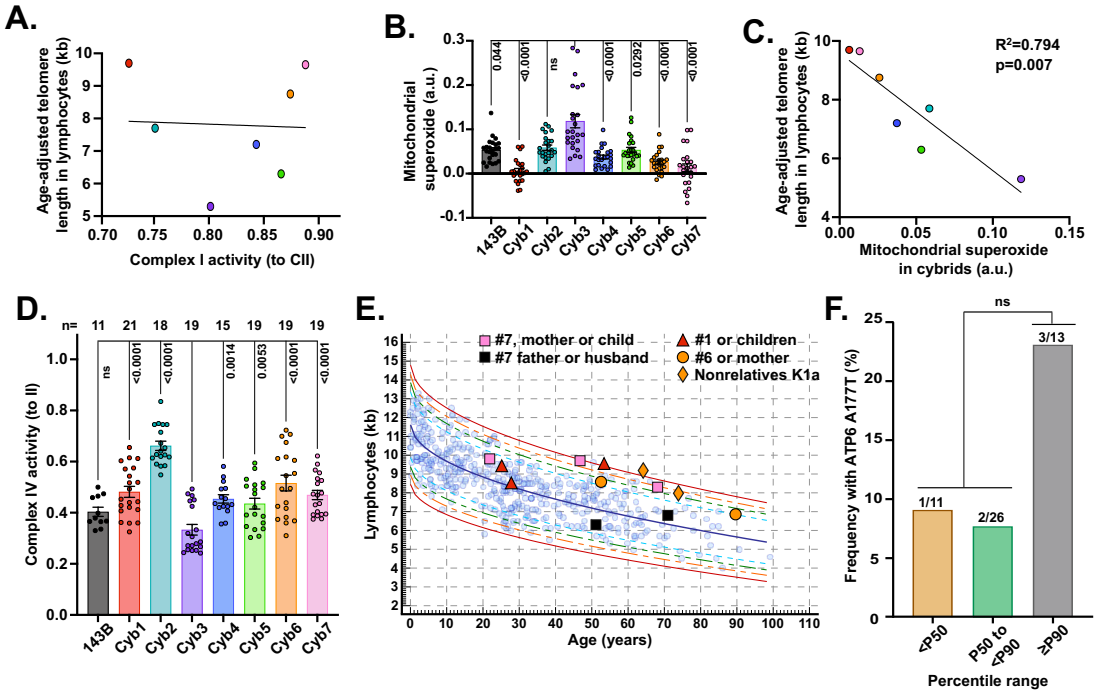
A.
Age-adjusted telomere length in lymphocytes (kb)
Complex I activity (to CII)
B.
Mitochondrial superoxide (a.u.)
0.044
<0.0001
ns
<0.0001
0.0292
<0.0001
<0.0001
143B
Cyb1
Cyb2
Cyb3
Cyb4
Cyb5
Cyb6
Cyb7
C.
R²=0.794
p=0.007
Age-adjusted telomere length in lymphocytes (kb)
Mitochondrial superoxide in cybrids (a.u.)
D.
n= 11 21 18 19 15 19 19 19
ns
<0.0001
<0.0001
0.0014
0.0053
<0.0001
<0.0001
Complex IV activity (to II)
143B
Cyb1
Cyb2
Cyb3
Cyb4
Cyb5
Cyb6
Cyb7
E.
#7, mother or child
#7 father or husband
#1 or children
#6 or mother
Nonrelatives K1a
Lymphocytes (kb)
Age (years)
F.
ns
3/13
1/11
2/26
Frequency with ATP6 A177T (%)
<P50
P50 to <P90
≥P90
Percentile range

685

686

687 **Figure 4. Mitochondrial superoxide production in cybrids inversely correlates with TL in**
688 **lymphocytes. A.** Lack of correlation between lymphocyte TL (in kb, adjusted to 50 yo) and average
689 CI activity measured in cybrids from the corresponding donors and normalized to CII activity
690 (CI/CII). **B.** Mitochondrial superoxide production measured by electron paramagnetic resonance
691 and corrected for background using PEG-SOD2 in clone #1 from all cybrids. n measurements from
692 2 biological replicates with 3 technical replicates. Mean ± SEM. Kruskal-Wallis test. ns: $p>0.05$. **C.**
693 Correlation between lymphocyte TL (in kb, adjusted to 50 yo) and average mitochondrial
694 superoxide production measured in cybrids from the corresponding donors. **D.** Complex IV activity
695 in 143B cells and in the cybrids. Values were normalized to CII activity. n measurements per cell
696 line from 2 biological replicates. One-way ANOVA. ns: $p>0.05$. **E.** TL of donor #7 (H1b1e), donor
697 #1 (T2b4a), donor #6 (K1a4a1) and their relatives is shown as indicated in the legend. Orange
698 triangles show TL in unrelated K1a11b and K1a4a1a2b donors. **F.** Frequency of donors with the
699 ATP6 A177T variant among n selected donors with lymphocyte TL in the indicated ranges (<P50,
700 between P50 and <P90 and ≥P90). Chi-square test.

701
702
703